51st AIAA/ASME/ASCE/AHS/ASC Structures, Structural Dynamics, and Materials Conference
 18th
12 - 15 April 2010, Orlando, Florida

AIAA 2010-2664

Pressure Adaptive Honeycomb: Mechanics, Modeling, and Experimental Investigation

Roelof Vos* and Ron Barrett†
The University of Kansas, Lawrence, Kansas

A new type of adaptive structure is presented that relies on a pressure differential to perform gross structural deformations. This structure relies on highly compliant honeycomb cells that can be pressurized externally or can rely on a pressure differential that exists at elevated altitudes. By pressurizing this honeycomb, its stiffness can be altered and deformations can be controlled by means of a restoring force. The mechanics of this pressure-adaptive honeycomb is laid out in this paper. The concept of equivalent material stiffness is introduced that assigns a Young's modulus to the honeycomb wall material that includes both the material-induced stiffness and the pressure-induced stiffness for a given cell differential pressure. The application of this model in a finite element analysis of a beam specimen is shown to correlate well to experimental results. In addition, the paper discusses possible applications for pressure adaptive honeycomb such as a Gurney flap and a solid-state flap. Wind tunnel test on a test article of a wing with pressure-adaptive flap demonstrates an increase in lift coefficient of 0.3 over a wide range of angles of attack. By increasing the pressure inside the flap to 40kPa its equivalent stiffness increases from 15kPa to 109kPa, thereby allowing the camber to decrease from 7.2% in deployed position to 2% in stowed position and shifting the point of maximum camber from 72% of the wing chord to 40%.

Nomenclature

E	Young's modulus, N/m^2
$\bar{E}$	Overall stiffness modulus of elasticity, N/m^2
$\bar{G}$	Overall hear modulus of elasticity, N/m^2
l	Wall length, m
m	mass, kg
p	Pressure, N/m^2
R	Specific gas constant, J/kg/K
t	Wall thickness, m
θ	Honeycomb angle, deg
σ	stress, N/m^2

Subscripts and superscripts

eq	equivalent
i	initial
lin	linearized
m	mass
p	pressure-induced
V	volume
x	longitudinal direction

*Assistant Professor, Faculty of Aerospace Engineering at Delft University of Technology, Kluyverweg 1, 2629HS Delft, The Netherlands, AIAA memeber
†Associate Professor, Department of Aerospace Engineering, 2120 Learned Hall, Lawrence, KS 66045, AIAA member

y lateral direction

Abbreviations

CDP	Cell Differential Pressure
FE	Finite Element
LSA	Light Sport Aircraft
SMA	Shape Memory Alloy

I. Introduction

The mission profile of a typical aircraft, ranging from light sport aircraft (LSA) to jet transports, requires the wing to adapt to the changing flight conditions. During cruise the wing shape is generally such that the lift-to-drag ratio is maximized. Typical characteristics for such a wing include minimal camber, small thickness-to-chord ratio, small surface area, and (possibly) high wing sweep. During landing the wing shape should be such that a maximum lift coefficient is obtained in order to comply with stall speed requirements and/or to minimize landing speed. This leads to contradictory requirements on the wing geometry such as high camber, large thickness-to-chord ratio, large surface area, and a low wing sweep. To comply with both requirements, aircraft have traditionally been equipped with high lift devices such as (multi-slotted) flaps and slats.

Another approach that has been taken in the past to satisfy these disparate requirements is altering the wing shape in a continuous manner, thereby creating so-called adaptive or morphing wings. Various examples of planform and section morphing wings have been shown over the past 100 years of flight. In the last decades morphing wing concepts have mainly concentrated on military aircraft and particularly on uninhabited aerial vehicles (UAVs).[1] An advantage that these classes of aircraft have over FAR 23, 25, 27, and 29 certified aircraft is that the materials that are employed to enable wing morphing are not required to be certified aerospace materials. This allows the use of adaptive materials such as shape memory alloys (SMAs) and piezoelectrics in primary and secondary structure. Commercial and general aviation aircraft cannot benefit from the use of these materials and a successful morphing wing for these aircraft classes should therefore be manufactured from certifiable aerospace materials.

For morphing wings it is generally acknowledged that a trade-off needs to be made between the stiffness of the wing and the amount of energy it takes to induce the required structural deformation. The mission adaptive wing (MAW^2), for example, used stout actuators that were heavy and bulky to induce the shape change in the wing. Another approach was taken during the active aeroelastic wing (AAW^3)program, where the aerodynamic forces were manipulated such that they induced favorable wing torsion. This successfully increased roll rates up to 400deg/s but with a more flexible wing that must have inherently led to lower flutter and divergence speeds. It would therefore be beneficial to have a wing that has significant stiffness during cruise (close to the maximum operating speed) such as to avoid these adverse aeroelastic effects. At the same time, it should be flexible enough during landing such as to allow for gross wing deformations.

Closely related to the stiffness of the morphing structure is the actuator selection and the energy requirement that stems from this selection. It can be easily deduced that the deformation of a stiff structure requires a large amount of mechanical energy. In conventional approaches this energy is extracted from sources within the aircraft. Whether it be electric, hydraulic, or pneumatic, each of these systems consumes power and requires wiring, piping, and/or tubing in order to function properly. A radically different approach to actuation of a morphing structure was demonstrated by Boeing in 2006.[5] They included SMA-actuated chevrons on the thrust-reverser sleeve of a 777 aircraft. Due to the change in ambient temperature between sea level and cruise altitude, these chevrons moved in and out of the engine exhaust (Fig. 1). At low altitudes the chevrons would be partially submerged in the exhaust, thereby decreasing the noise level and the efficiency of the engine. During cruise, they would open up and the engine would perform at maximum efficiency. This completely autonomous approach required no energy from aircraft sources but relied solely on the ambient temperature change.

Since SMA cannot be used in primary or secondary structure due to FAR 23/25 certification limitations, this application cannot be extrapolated to morphing wing structures. Other temperature-sensitive adaptive

(a) Covers Removed (b) Thrust Reverser Installed

Figure 1. Boeing's SMA Variable Geometry Chervrons[4]

structures can be devised that do consist of certified aerospace materials. One can think of laminates consisting of aluminum and carbon fibre, with a large discrepancy in coefficient of thermal expansion. A temperature change would hence induce bending in the laminate. However, this requires a very reliable temperature stimulus and both the atmospheric temperature change and aerodynamic heating need to be well established before designing such a structure. A brief study into the atmospheric composition and its seasonal and latitudinal deviation revealed that ambient pressure (contrary to ambient temperature) is a very reliable stimulus for an adaptive structure. As can be seen from Figure 2, the summer pressure and winter pressure show very minor deviation. The latitudinal deviation is also relatively small. This makes ambient pressure a much more reliable stimulus than ambient temperature.

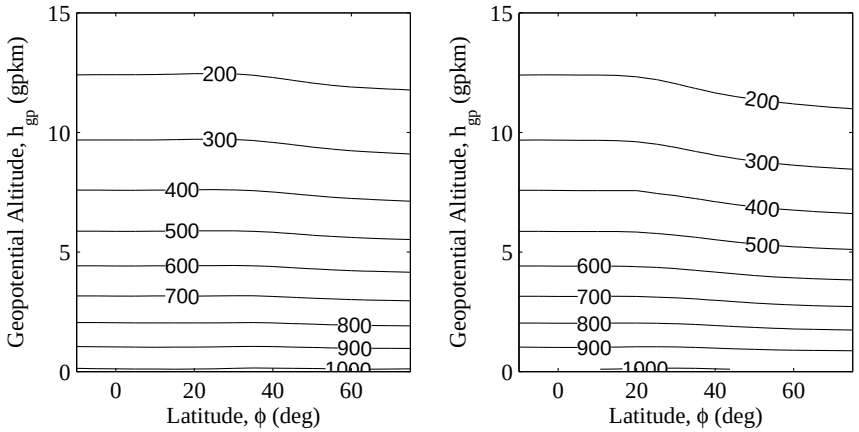

(a) Summer Pressure, p_a (hPa) (b) Winter Pressure, p_a (hPa)

Figure 2. Isobars for Mean Winter and Summer Atmospheric Conditions[6]

In this article a new adaptive structure is presented that addresses each of the discussed items from the previous paragraphs. This adaptive structure relies on pressurized honeycomb cells. These honeycomb cells extend a significant amount perpendicular to the plane of the hexagons. In each cell resides a pouch (bladder) that can be pressurized. Pressurizing the pouches increases the stiffness of the honeycomb. When an external force field is present and the pouches are unpressurized, the honeycomb can be substantially deformed. A subsequent increase in pressure results in a geometry of the honeycomb where the cells assume a shape that is close to a perfect regular hexagon. Figure 3 schematically demonstrates how these large strains can be attained without plastically straining the cell walls. Two cases are depicted where different initial manufacturing shapes are assumed. At elevated cell differential pressure (CDP) both cells converge

to a close-to regular hexagonal shape. Longitudinal strains in excess of 50% can be attained while lateral strains in excess of 70% can be obtained, where the strain is measured with respect to the dimensions of perfect hexagonal shape (CDP$\rightarrow \infty$).

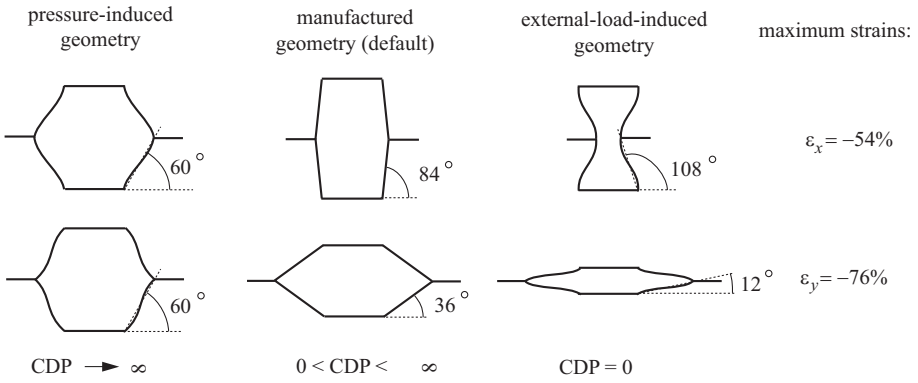

Figure 3. Maximum Deformations of Pressure Adaptive Honeycomb

The pressure adaptive honeycomb structure can be manufactured from conventional aerospace materials such as aluminum or composites. The pouches inside can be made from an aerospace grade of nylon. From a material point of view, this structure could, therefore, be applied to FAR 23, 25, 27, and 29 certified aircraft. In addition, the stiffness can be tailored such that at high speeds, the pressurized honeycomb becomes relatively stiff, thereby avoiding any adverse aeroelastic effects. At landing conditions, the stiffness can be lowered and an externally applied load can create the required structural deformation. This structure also allows for autonomous operation when each of the pouches that reside inside the cells are filled with a constant amount of air. The pressure-altitude relation can then be employed as a trigger mechanism to induce deformation between landing and cruise conditions.

This paper presents the mechanics of pressurized honeycomb and introduces a mathematical model that forms a basis for future modeling of complex, pressure adaptive structures.

II. Mechanics of Pressure Adaptive Honeycomb

In this section two separate mathematical models are presented. One for the standard honeycomb (non pressurized) and one for a simplified pressure-adaptive honeycomb. Each of these models predicts a stiffness modulus. It is subsequently assumed that the material-induced stiffness and pressure-induced stiffness are independent of each other and can therefore be added. The resulting nonlinear analytical model can be used to predict the stress strain relations when loading in principal direction is applied and the honeycomb is free to contract or expand in the direction perpendicular to loading. Subsequent simplifications are made such that an equivalent model can be employed in a finite element analysis. Figure 4 schematically shows the evolution of the model. In the following subsection reference is made to this flow chart and the underlying assumptions are explained.

A. Mechanics of Plain Honeycombs

The mechanics of honeycombs have been investigated for more than twenty years and are well understood. Principal loading of a honeycomb structure induces wall deformations, such as schematically shown in Figure 5. The diagonal walls display an (inverse) s-shape, while the horizontal member remains unstrained. Following the cellular material theory (CMT) laid out by Gibson and Ashby,[7] the overall stiffness moduli ($\bar{E}_x^m$, $\bar{E}_y^m$, $\bar{G}_{xy}^m$) can be expressed as a function of the thickness-to-length ratio (t/l), the initial honeycomb angle (θ_i), and the material's Young's modulus (E^m). This yields constant overall stiffness moduli that can be

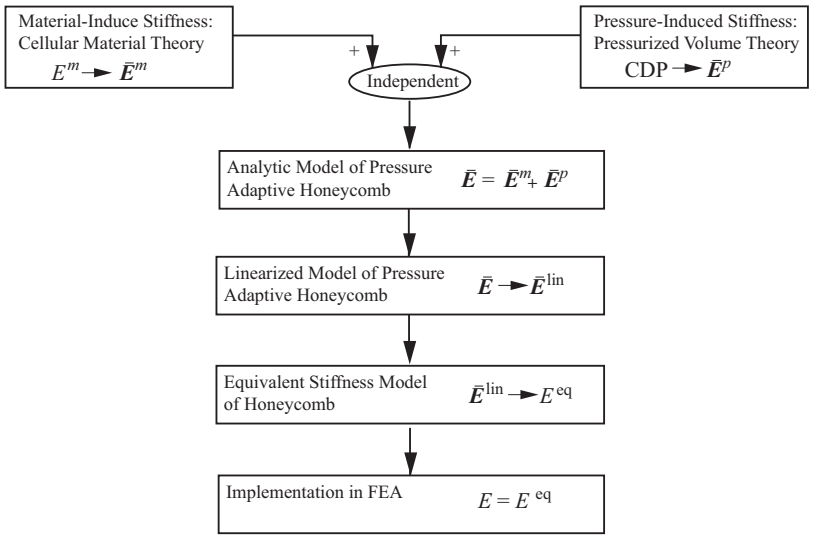

Figure 4. Flow Chart of Pressure Adaptive Honeycomb Modeling

employed to predict a linear stress-strain in principal direction when no boundary conditions are specified:

$$\bar{E}_x^m = E^m \left(\frac{t}{l}\right)^3 \frac{\cos\theta_i + 1}{\sin^3\theta_i} \tag{1}$$

$$\bar{E}_y^m = E^m \left(\frac{t}{l}\right)^3 \frac{\sin\theta_i}{(\cos\theta_i + 1)\cos^2\theta_i} \tag{2}$$

$$\bar{G}_{xy}^m = E^m \frac{4}{5} \left(\frac{t}{l}\right)^3 \frac{\cos\theta_i + 1}{\sin\theta_i} \tag{3}$$

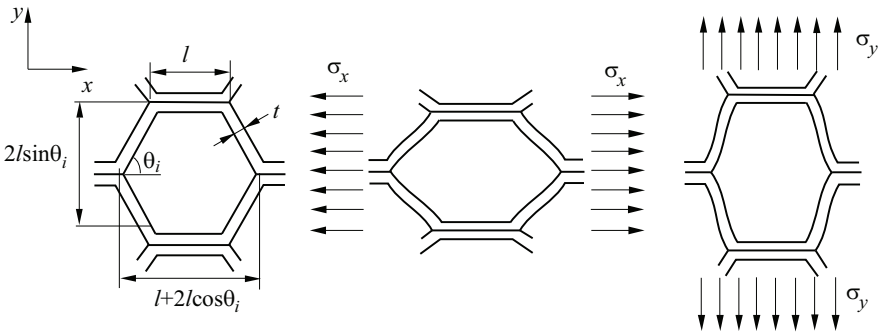

Figure 5. Cell Deformation due to Stresses in Principal Directions

B. Mechanics of Pressurized Rigid-Wall Honeycomb

When honeycomb is pressurized it shows a higher resistance against deformation, i.e. the stiffness is increased. Similar to any other pressurized volume (e.g. a cylinder/piston combination), a change in volume can be used to extract mechanical work. The useful work that can be obtained when a pressurized initial volume, V_i, is expanded to a new volume, V, can be described as:[8]

$$W_{use} = \int_{V_i}^{V} p\mathrm{d}V - p_a(V - V_i) \tag{4}$$

where p is the pressure inside the volume and p_a is the ambient pressure. The integral can be expanded under two assumptions that can be associated with two different applications of pressure adaptive honeycomb. Under the first assumption, the pressure, p inside the honeycomb is held constant. This would correspond to an application where the pilot controls the pressure inside the honeycomb. Under the second assumption the mass, m is held constant and the perfect gas law is employed, i.e. $p = mRT/V$. This would correspond to the case where the pressure adaptive honeycomb is completely autonomous and relies on the ambient pressure, p_a, to create useful work.

The useful work can, in turn, be employed to do external work:

$$W_{ex} = \int_{s_i}^{s} F \mathrm{d}s \tag{5}$$

It is assumed that the pressurized volume, i.e. the honeycomb cells, can be approximated by a structure of rigid members connected by frictionless hinges. By equating Eqs. 4 and 5 and relating the volume V to the displacement s via the honeycomb angle, θ, a closed-form relation between displacement and force can be established. This relation can be rewritten to form nonlinear stress-strain relations in the principal directions. The corresponding stiffness moduli are denoted $\bar{E}_x^p(\epsilon_x, \theta_i)$, $\bar{E}_y^p(\epsilon_y, \theta_i)$, $\bar{G}_{xy}^p(\gamma_{xy,\theta_i})$.

C. Mechanics of Pressure Adaptive Honeycomb

The stiffness of a pressure adaptive honeycomb is composed of the stiffness induced by the honeycomb material and the pressure-induced stiffness. To model the stiffness of pressure adaptive honeycomb it is assumed that these two stiffnesses are independent and can therefore be added. If the stiffness definitions from the previous subsections are used, the stress-strain relations in principal directions (without the enforcement of boundary conditions) can be expressed as:

$$\sigma_x = \left[\bar{E}_x^p(\epsilon_x, \theta_i) + \bar{E}_x^m(t/l, E^m, \theta_i)\right] \epsilon_x \tag{6}$$

$$\sigma_y = \left[\bar{E}_y^p(\epsilon_y, \theta_i) + \bar{E}_y^m(t/l, E^m, \theta_i)\right] \epsilon_y \tag{7}$$

$$\tau_{xy} = \left[\bar{G}_{xy}^p(\gamma_{xy}, \theta_i) + \bar{G}_{xy}^m(t/l, E^m, \theta_i)\right] \gamma_{xy} \tag{8}$$

These relations form the analytical model which forms the foundation of the linearized model that is described in the next subsection. These relations hold for large strains.

D. Equivalent Stiffness Approach of Pressure Adaptive Honeycomb

The analytical model that describes the stress-strain relations of pressurized honeycomb cannot be used in a finite element analysis due to the fact that no boundary conditions or complex loading conditions can be included. To that extent an equivalent pressure adaptive honeycomb model is developed based on the relations of Eqs. 6, 7, and 8, and the dimensions of regular non-pressurized honeycomb. To achieve the equivalent representation the nonlinear stress strain relations are first linearized with respect to the position of zero strain. This results in the following set of equations:

$$\sigma_x^{\mathrm{lin}} = \left[\bar{E}_x^p(\theta_i) + \bar{E}_x^m(t/l, E^m, \theta_i)\right] \epsilon_x \tag{9}$$

$$\sigma_y^{\mathrm{lin}} = \left[\bar{E}_y^p(\theta_i) + \bar{E}_y^m(t/l, E^m, \theta_i)\right] \epsilon_y \tag{10}$$

$$\tau_{xy}^{\mathrm{lin}} = \left[\bar{G}_{xy}^p(\theta_i) + \bar{G}_{xy}^m(t/l, E^m, \theta_i)\right] \gamma_{xy} \tag{11}$$

Of course, this also implies the effect of deformation on θ_i is "small," generally in line with an infinitesimal strain assumption. In Figures 6(a) and 6(b) the difference between the analytical and linearized stress strain model is demonstrated for the case of an assumed constant mass (Fig. 6(a)) and for the case of controlled constant pressure (Fig. 6(b)). In the latter figure, the cell differential pressure (CDP) is defined as CDP$= p - p_a$. It can be seen that at higher strains the deviation between the linear and nonlinear model increases. For the case of a constant CDP, the linearized model is accurate within 5% under the following stain conditions: $-4.5\% < \epsilon_x < 4.5\%$ and $-2.5\% < \epsilon_y < 2\%$

The linearized model forms the basis of the equivalent stiffness model, where the honeycomb material is assigned a new Young's modulus that accounts for both the material stiffness and the pressure-induced stiffness. The advantage of such an equivalent model is that the mechanics of the pressure-adaptive honeycomb

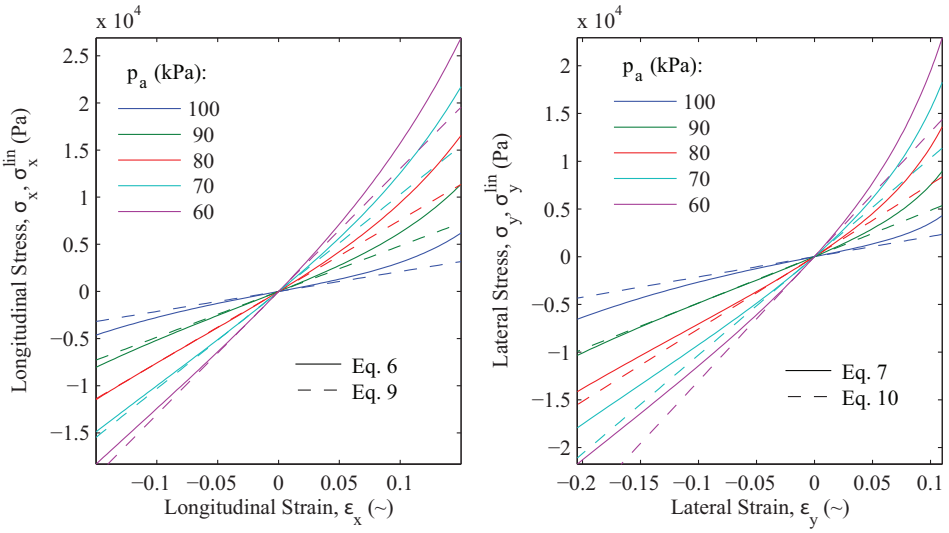

(a) Assumption: Constant Mass ($mRT/V_i = 100$kPa)

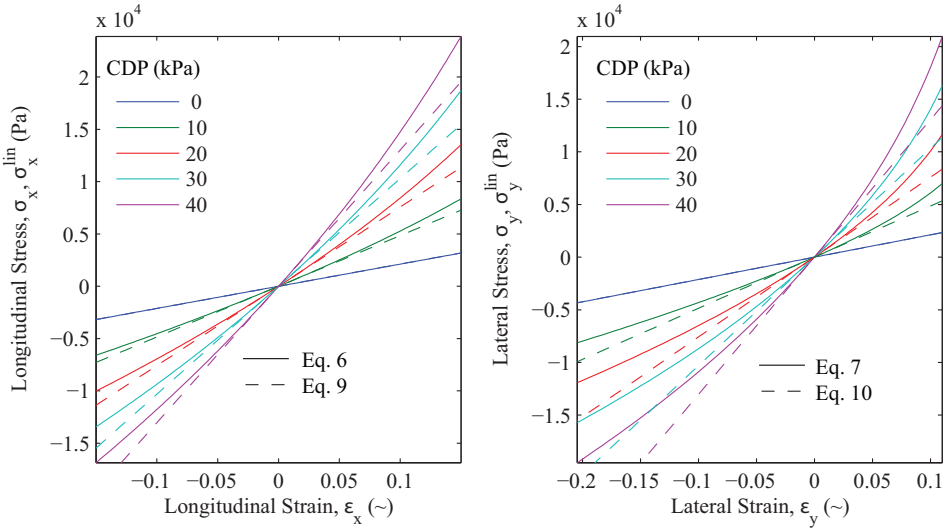

(b) Assumption: Constant Pressure

Figure 6. Comparison between Principal Stresses as Predicted by Analylical Model and Linearized Model

are properly captured while the individual pouches do not need to be explicitly defined. Therefore, it is less complicated to design a pressure-adaptive structure and evaluate its properties.

If the vector of linear overall stiffness moduli is denoted with $\bar{\mathbf{E}}^{\text{lin}}$ then the following is implied: $\bar{\mathbf{E}}^{\text{lin}} = \bar{\mathbf{E}}^{p}(\theta_i) + \bar{\mathbf{E}}^{m}(t/l, E^m, \theta_i)$. The equivalent Young's modulus, E^{eq}, of the honeycomb can be found from each of the three gross stifnesses in $\bar{\mathbf{E}}$ using CMT in an inverse manner:

$$E^{\text{eq}} = \bar{E}_x^{\text{lin}} \left(\frac{l}{t}\right)^3 \frac{\sin^3\theta_i}{\cos\theta_i + 1} \tag{12}$$

$$E^{\text{eq}} = \bar{E}_y^{\text{lin}} \left(\frac{l}{t}\right)^3 \frac{(\cos\theta_i + 1)\cos^2\theta_i}{\sin\theta_i} \tag{13}$$

$$E^{\text{eq}} = \bar{G}_{xy}^{\text{lin}} \frac{5}{4} \left(\frac{l}{t}\right)^3 \frac{\sin\theta_i}{\cos\theta_i + 1} \tag{14}$$

A more elaborate derivation of the equivalent material stiffness of pressurized honeycomb can be found in Vos.[9] The equivalent stiffness that has been derived above can subsequently be used in a finite element analysis of a pressure adaptive honeycomb structure. It can be observed from Eqs. 12 through 14 that determining the overall stiffness in one of the principal directions or in the shear direction can directly be used in the calculations of the equivalent Young's modulus of the structure.

III. Experimental Results and Correlation to Theory

To test the validity of the analytic model and the equivalent stiffness model, two series of tests were carried out. The first set of tests were used to demonstrate that the analytical model correlated to the experimental results, while the a second test was carried out to demonstrate that the equivalent stiffness model could be used to predict the mechanical behavior of a more complicated pressure adaptive honeycomb structure. These tests are described in the subsequent subsections.

A. Uniform Loading in Principal Stress Directions on Bulk Specimen

A 130-cell pressure adaptive honeycomb structure was subjected to uniform compression loading in longitudinal (x-) and lateral (y-) direction. A uniform stress was induced in these principal directions. Boundary conditions allowed for (almost) free expansion in the direction perpendicular to loading. Each of the cells was individually pressurized and kept at a constant CDP. During the test force and displacement were recorded, from which stress and strain could be calculated. Figures 7(a) and 7(b) present the experimentally obtained results and the prediction. On the vertical axes, the stress is normalized with respect to the applied pressure, p.

From Figs. 7(a) and 7(b) it can be seen that the analytical model correlates well to the experimental results. It can also be seen that the model underpredicts in case of longitudinal compression and overpredicts in case of lateral compression. These discrepancies are thought to be caused by manufacturing imperfections, where the real honeycomb geometry deviated locally from the assumed geometry in the model.

B. Three-Point Bend Test on Beam Specimen

To investigate the predictive capability of the equivalent stiffness model, a 145-cell honeycomb beam structure was constructed. The honeycomb was then rigidly attached to a flat aluminum plate, which, in turn, was subjected to a three-point bend test (see Fig. 8). The specimen was tested at various CDPs and force and displacement were recorded during the test. In Figure 9 it can be seen that the prediction of the finite element analysis (FEA) with the equivalent stiffness model correlated very well to the experimental results at the two CDPs. Similar correlations were found at 5 and 20kPa, but are not shown here for the sake of brevity. Because the specimen did not encounter any large cell strains, the small-strain assumption of the linearized model was valid in this case. This test demonstrated that the equivalent stiffness model could be used to predict the mechanical properties of the pressure adaptive honeycomb.

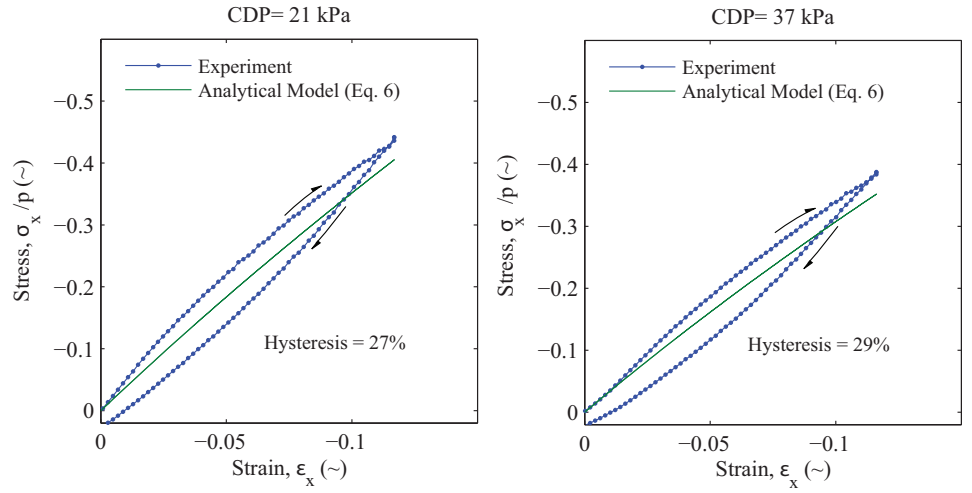

(a) Longitudinal Compression

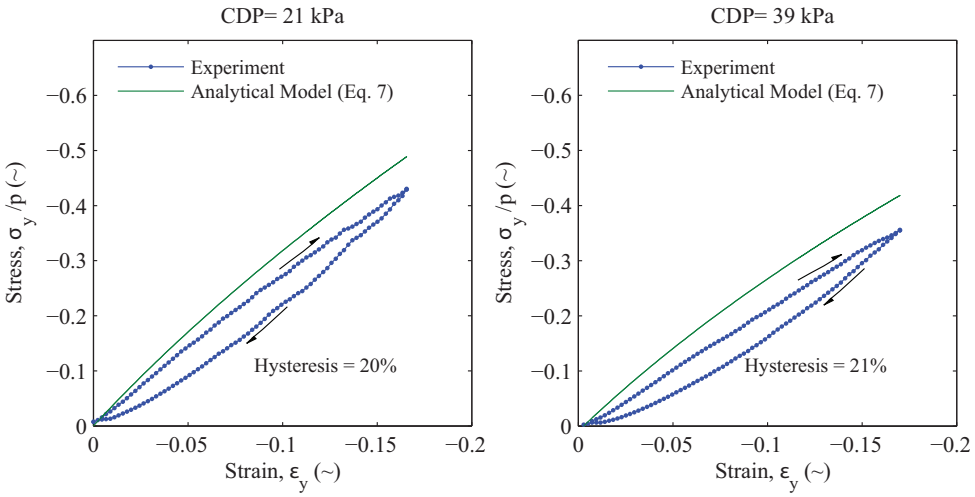

(b) Lateral Compression

Figure 7. Results of and Correlation Compression Tests

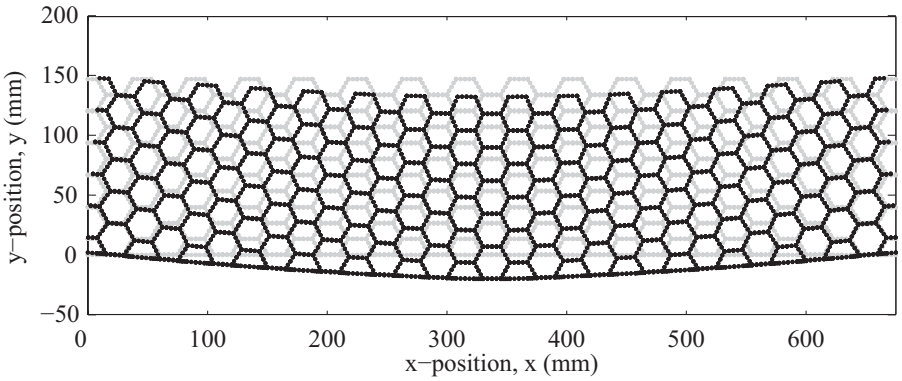

Figure 8. FEA Result of Three-Point Bend Test

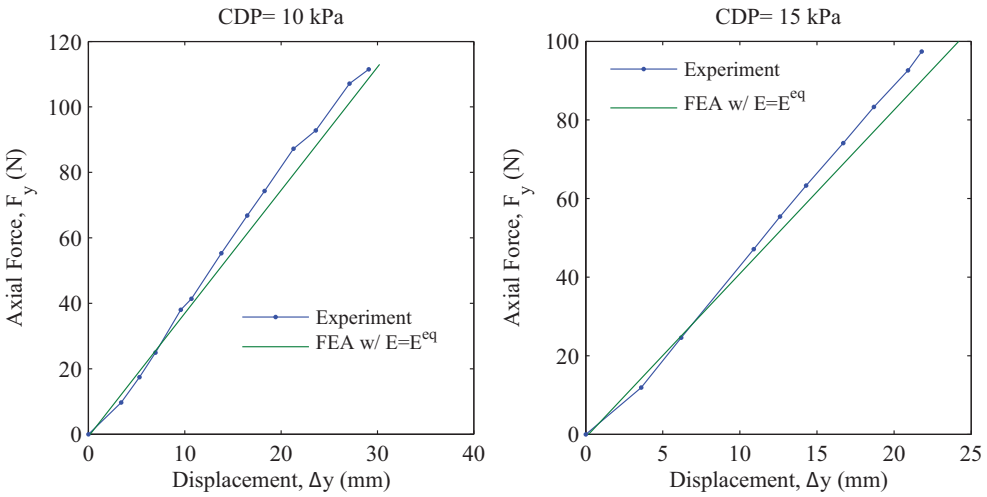

Figure 9. Results of Three-Point Bend Test and Correlation to FEA Results

IV. Application of Pressure Adaptive Honeycomb

The mission profile of a typical jet transport leads through a significant change in ambient pressure. A pressure difference as high as 80kPa can be encountered between take-off and cruise. The difference between cabin and ambient pressure results in an effective stiffening of the fuselage structure. In a similar, but more profound manner the change in ambient pressure can be employed to actuate a pressure-adaptive structure through a natural coupling between a pressure differential and structural stiffness. The application and potential operation of such a structure is covered in this section.

A. Example I: Gurney Flap for Jet Transports and Business Jets

Based on the principle of variable stiffness of pressure adaptive honeycomb and its simple incarnation to straighten initially curved plates, a proof-of-concept demonstration article was conceived. A pressure-adaptive Gurney flap was designed that could potentially be used to increase the maximum lift coefficient on a jet transport or business jet. Gurney flaps have been shown to increase $c_{l_{max}}$ on single slotted wings up to 20%.[10] However, during cruise they produce unwanted profile drag. A pressure adaptive Gurney flap would therefore be a desirable addition to conventional high-lift devices. Such a pressure adaptive Gurney flap could replace a conventional trailing edge on a business jet or a jet transport as is schematically shown in Figure 10.

In the demonstration article the pressure adaptive honeycomb was stretched and bonded to the pre-curved bottom skin of the Gurney flap. The upper skin was also pre-curved and could slide with respect to the honeycomb and the bottom skin (see Figure 11). In each of the honeycomb cells a simple mylar pouch was inserted that was filled with a constant amount of air and appropriately sealed. The deployed pressure adaptive Gurney flap was subsequently positioned in a transparent vacuum chamber. The vacuum chamber imitated the ambient pressure drop that would be typically encountered by a jet transport or business jet. As can be seen from the difference between the two shapes in Figure 11 a pressure decrease of 80kPa ensured almost complete stowage of the pressure adaptive Gurney flap. This demonstrated the operating principle of an autonomous pressure adaptive structure.

B. Example II: Solid State Flap for Light Sport Aircraft

Light sport aircraft (LSA) need to comply with a 45kts clean wing stall requirement which dictates the sizing of the wing. A pressure adaptive wing could assist in compliance with this requirement for a smaller and, hence, more efficient wing. Replacing the conventional flap structure with a pressure-adaptive honeycomb flap can autonomously adjust the camber over the aft portion of the wing. Alternatively, a pressure adaptive droop nose could be constructed or a combination of both. Such an autonomous camber change could

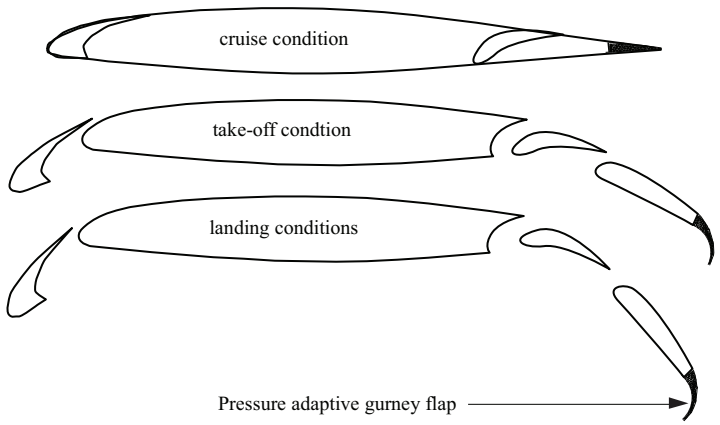

Figure 10. Sketch of Application of Pressure Adaptive Honeycomb on a 5%c Gurney Flap

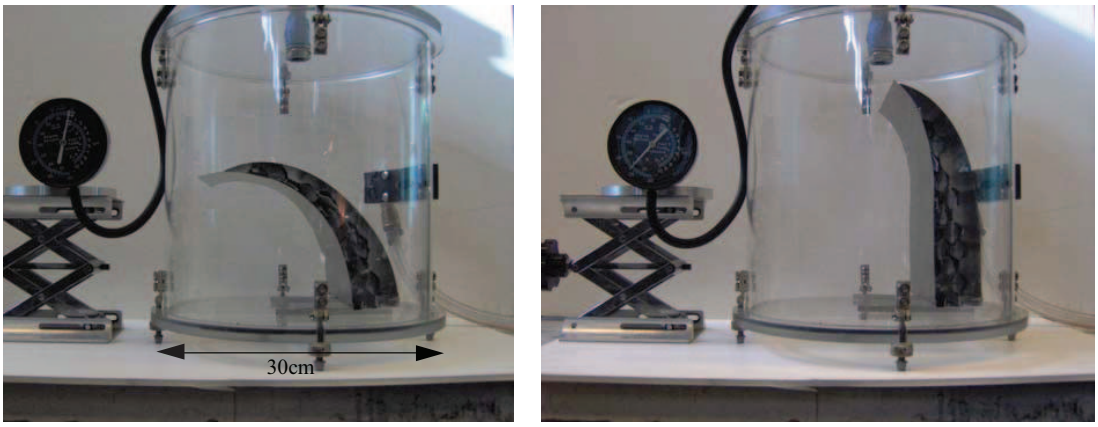

Figure 11. Pressure Adaptive Gurney Flap in Deployed (left) and Stowed (right) Position

increase the maximum lift coefficient during take-off and landing conditions such that the total planform area can be reduced for the same landing performance. A schematic design of such a pressure adaptive LSA wing is depicted in Figure 12. In this concept also drooped ailerons are envisioned, which ensures an even higher lift increase over the entire span of the aircraft.

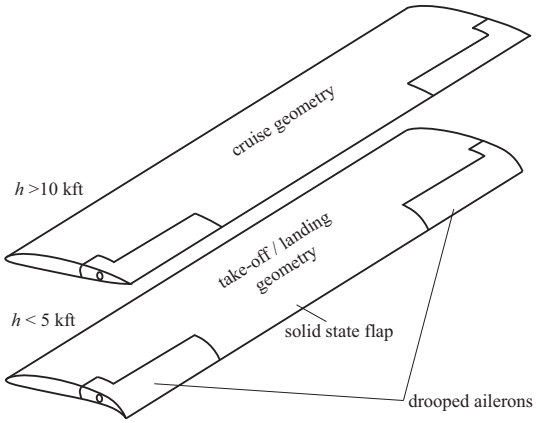

Figure 12. Sketch Solid State Pressure Adaptive Gurney Flap on LSA wing

A section of an LSA wing with a pressure adaptive flap was constructed to demonstrate the effectiveness of such a concept in the wind tunnel. In Figure 13 the wind tunnel model is shown in the low speed wing tunnel of The University of Kansas. A distinct camber change can be observed between the deployed flap (left) and the stowed flap (right). This geometry change was induced by applying a 40kPa CDP. By increasing the pressure inside the flap to 40kPa its equivalent stiffness increased from 15kPa to 109kPa. The model was based on a NACA 2412 airfoil and had pressure adaptive flap over the aft 32% of the wing chord. Pressurizing the honeycomb resulted in the camber to decrease from 7.2% in deployed position to 2% in stowed position and shifting the point of maximum camber from 72% of the wing chord to 40%. Wind tunnel tests were carried out at wind speeds of 30, 45, and 60kts and angles of attack ranging from -6° to 20°. In post-processing the results wind tunnel wall corrections were applied according to the methods laid out in Barlow et al.[11]

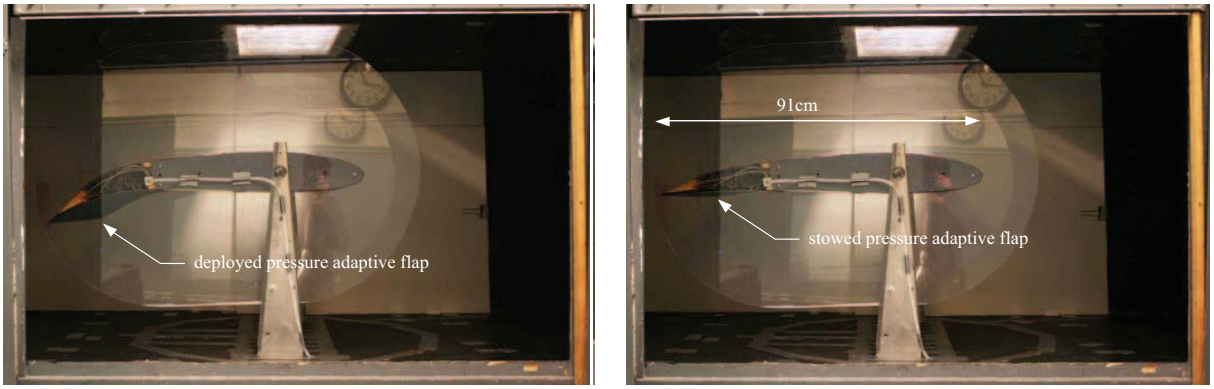

Figure 13. Wind Tunnel Model with Deployed (left, CDP = 0) and Stowed (right, CDP = 40kPa) Pressure Adaptive Flap

During the wind tunnel tests the lift, drag and moment coefficient about the quarter chord point were measured. In Figure 14) the lift coefficient as a function of CDP is presented for various (corrected) angles of attack and the three speeds. It can be seen that throughout the range of angles of attack the effect of wing morphing was largest for the lowest speed and hence dynamic pressure. For a corrected speed of 32

kts it can be seen that a change in lift coefficient of 0.3 could be obtained between deployed and stowed flap. This number was approximately halved for speeds twice as large ($\Delta c_l \approx 0.15$ at 64kts). At 32 kts an increase in lift coefficient from 1.23 to 1.53 was measured at an angle of attack of 21 degrees by deploying the pressure adaptive flap. At higher velocities the higher dynamic pressure induced an upward deflection of the flap when no CDP was applied. This was a result of the flexibility of the flap, which did not scale with the dynamic pressure. This also demonstrates that in future designs the flexibility of the flap should be tailored to the speed at which it will be deployed.

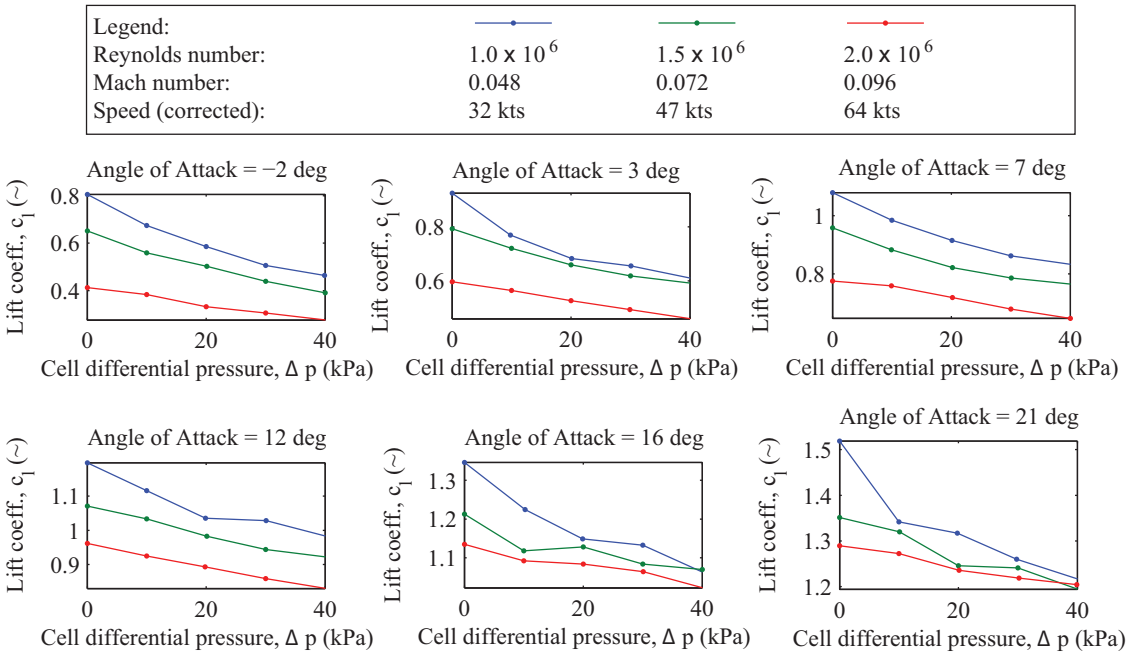

Figure 14. Lift Coefficient versus CDP for Various (Corrected) Angles of Attack and Reynolds/Mach Numbers

Although LSA aircraft do not experience the same pressure differences during their mission profile as jet transports or business jets, the relatively large pressure gradient in the lower layers of the atmosphere can still be employed to induce gross wing deformations in favor of a higher (flaps-up) maximum lift coefficient. Increased nose-down moment due to the autonomous deployment of the pressure adaptive flap can be balanced by a pressure-adaptive trim tap or equivalent pressure adaptive structure in the horizontal stabilizer.

V. Conclusions and Future Work

A new pressure adaptive structure has been presented based on a pressurized honeycomb. Such a pressure adaptive honeycomb can be employed in airplanes ranging from light sport aircraft to jet transports. It has been shown that a pressure adaptive Gurney flap can be constructed that is deployed near sea level but retracts as the ambient pressure decreases. In addition, it has been demonstrated how a pressure adaptive wing on a light sport aircraft would increase the lift coefficient by 0.3, thereby reducing the required wing surface area to comply with the 45kts stall requirement, resulting in a more efficient wing during cruise conditions. By increasing the pressure inside the flap to 40kPa its equivalent stiffness increased from 15kPa to 109kPa, thereby allowing the camber to decrease from 7.2% in deployed position to 2% in stowed position and shifting the point of maximum camber from 72% of the wing chord to 40%. An analytical model has been derived based on the conservation of mechanical energy assumption that describes the relation between the pressure in the honeycomb, the applied stress, and the resulting strain. This model has been shown to predict the stress-strain behavior of pressure adaptive honeycomb to strains up to -17%. An equivalent stiffness model has been subsequently derived that substitutes the value of the Young's modulus of the honeycomb material with a one that includes the effect of pressurization on the bulk of the material. This

model has been shown to accurately predict the mechanical behavior of a constrained honeycomb beam in a three-point bend test. Future endeavors should be concentrated on expanding the equivalent stiffness model such that it can be employed for the prediction of even larger deformations that are associated with the application of pressure adaptive honeycomb in a morphing wing structure.

Acknowledgements

The authors wish to acknowledge the generous support of the University of Kansas Transportation Research Institute (TRI) and the Aerospace Engineering Department for funding this research. In addition, the authors wish to acknowledge the support from Prof. Karan S. Surana and Prof. Albert Romkes, Mechanical Engineering Department, University of Kansas, for providing the FE program FINESSE to perform the FE computations in this work. The authors would also like to recognize Ms. Lauren Kerth, Mr. Thomas Stastny and Mr. Ryan Barnhart for their tireless efforts in assisting fabricating the test articles.

References

[1]Akhilesh, K. and Kudva, J., "Morphing Aircrat Concepts, Classification, and Challenges," *SPIE Smart Structures and Materials Conference*, edited by E. H. Anderson, Vol. 5388, SPIE, San Diego, 2004.

[2]Gould, D. K., "Mission Adaptive Wing Flight Demonstration Program," *SAE Aerospace Congress & Exposition*, SAE-811035, Anaheim California, 1981.

[3]Pendleton, E., Bessett, D., Field, P., Miller, G., and Griffin, K., "Active Aeroelastic Wing Flight Research Program: Technical Program and Model Analytical Development," *Journal of Aircraft*, Vol. 37, No. 4, 2000, pp. 554–561.

[4]Calkins, F. T. and Butler, G. W., "Variable Geometry Chevrons for Jet Noise Reduction," *12th AIAA/CEAS Aeroacoustics Conference*, AIAA Paper 2006-2546, Cambridge, Massachusetts, 2006.

[5]Turner, T. L., Buehrle, R. D., Cano, R. J., and Fleming, G. A., "Modeling, Fabrication, and Testing of a SMA Hybrid Composite Jet Engine Chevron Concept," *Journal of Intelligent Material Systems and Structures*, Vol. 17, 2006, pp. 483–497.

[6]Oort, A. H. and Rasmusson, E. M., "Atmospheric Circulation Statistics," Tech. Rep. Professional Paper 5, US Deparment of Commerce, National Oceanic and Atmospheric Administration, September 1971.

[7]Gibson, L. J. and Ashby, M. F., *Cellular Solids, Structure and Properties*, Cambridge University Press, 1st ed., 1988.

[8]Rolle, K. C., *Thermodynamics and Heat Power*, Pearson Prentice Hall, Upper Saddle River, NJ, 6th ed., 2005.

[9]Vos, R., *Mechanics and Applications of Pressure Adaptive Honeycomb*, Ph.d. thesis, The University of Kansas, Department of Aerospace Engineering, Lawrence, KS, Septemeber 2009.

[10]Katz, J. and Largman, R., "Effect of 90 Degree Flap on the Aerodynamics of a Two-Element Airfoil," *Journal of Fluid Engineering*, Vol. 111, 1989, pp. 93,94.

[11]Barlow, J. B., Rae, W. H., and Pope, A., *Low-Speed Wind Tunnel Testing*, Wiley & Sons, New York, 3rd ed., 1999.